Student Project

Comparison of Highly Compact Interleaved 48V-12V DC-DC Converters for Vehicle Systems

by

Felix Johann Hahn, Shobhit Ramkripal Sharma

Matriculation No. 7010108, 6898232

in partial fulfillment of the requirements for the degree

Master of Science

(M. Sc.)

at the department

Power Electronics and Electrical Drives

Supervisors: Nikolas Förster, Philipp Rehlaender
Examiner: Prof. Dr.-Ing. Joachim Böcker
Date: Paderborn, January 15, 2022

CONTENTS

LIST OF FIGURES

LIST OF TABLES

INTRODUCTION

The current trend in Automotive industry is to convert into hybrid or fully electric vehicle systems. One of the fundamental changes in this direction is, perhaps, the installation of 48 V DC systems alongside the existing 12 V DC systems. A way to connect these two voltage levels together is by using a DC-DC converter.

Previous project groups focused on the design and optimization of a 1 kW DC-DC converter with coupled magnetics. In line with that, a redesign of the 1 kW converter was done in WS19/20. The assembly began in SS20 and got completed in WS20/21. The first measurements were also taken in WS20/21. A new 2 kW DC-DC converter was designed, first time, with pairwise coupled inductors in SS20. The design of PCB and inductors were completed in WS20/21. The assembly was also started in WS20/21 but could not be completed due to the COVID-19 pandemic. Considering the project history of the present converters, the 1 kW converter corresponds to version 10.0 and the 2 kW converter to version 11.0.

This project analyses these two 48 V to 12 V bidirectional DC-DC converters designed by the previous project groups. The two DC-DC converters are shown in Figure 1.
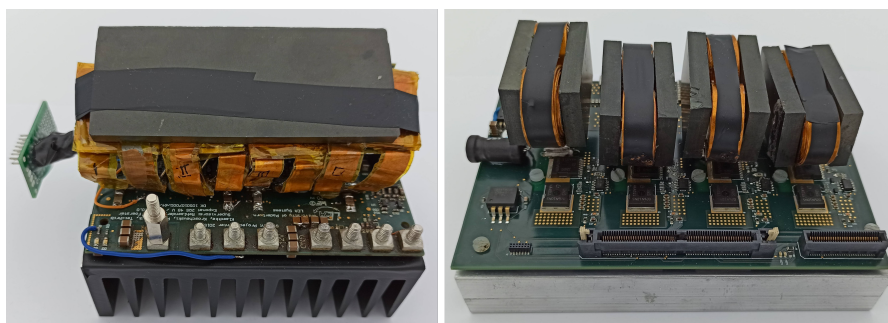
Figure 1: Prototypes of the 1 kW converter (left) and 2 kW converter (right)

1.1 TASK DESCRIPTION

The assembly and testing of the 2 kW converter is done in this project. Assembly contains manufacturing of coils and heat sink, testing of control, soldering a second PCB. After a successful operation of the 2 kW converter, the focus of this project is also to compare the two converters shown in Figure 1.

This report is divided into four chapters based on the goals described above. Chapter 2 and Chapter 3 are devoted to the comparison of the two converters. The first chapter presents in detail, the major design differences. These comprises of topology used, MOSFETs type and inductor design. In addition to that, the power density is analyzed. Whereas, the second chapter compares the two converters based on their measurement results (performance), such as efficiency and thermal profile. To compare the hardware design of the converters, control algorithm and cooling system is kept same except for some required small changes. This chapter also describes the test setup and measurement procedure.

As the previous project group could not test the 2 kW converter due to the COVID-19 pandemic, it is assembled and tested in this project. The process of assembly and the problems encountered during this phase are explained in Chapter 4. Soldering issues, heating of capacitors, and design discrepancies are some of the difficulties which are documented in this chapter.

Chapter 5 gives a short overview of the control architecture employed. The code of the WS19/20 project group was used as the basis for the microcontroller firmware in both the converters. The TMDSC-NCD28335 control card is used for the 1 kW converter control while for the 2 kW converter, a new control card is used. The new control card (TMDSDOCK28379D) is based on the TMS320F28379D microcontroller which is significantly different from the TMS320F28335 microcontroller.

DESCRIPTION OF THE 1 KW AND 2 KW CONVERTER

This chapter is intended to provide an overview of both converters. Therefore, the basic topology of the converters is presented first. Subsequently, the most important hardware differences between the 1 kW and the 2 kW converter are described. The power density is also considered.

2.1 TOPOLOGY

The 1 kW and the 2 kW converter are both bidirectional 4 times interleaved DC-DC converters. The topology of the 1 kW converter is shown in Figure 2. The circuit consists of four bidirectional DC-DC converters connected in parallel and driven by phase-shifted (90°) gate signals. The converters can be operated in buck mode as well as in boost mode. The topology of the 2 kW converter is almost identical, but it contains pairwise coupled inductors for each half bridge. This topology can be found in Appendix A. A detailed explanation of a bidirectional DC-DC converter can be found in [4].
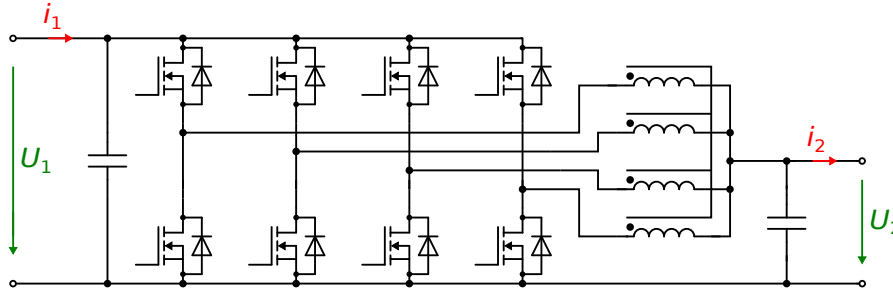
Figure 2: 4 times interleaved topology of the 1 kW converter with coupled inductors, $U_1 = 48\,\text{V}$ and $U_2 = 12\,\text{V}$

2.2 DESIGN DIFFERENCES

The most important hardware differences between the 1 kW and the 2 kW converter are found in inductors, MOSFETs and control cards. These differences are summarized in the following.

- **Inductors**
  The 1 kW converter makes use of inductors that share the same core and are therefore coupled. The windings are of rectangular shape in order to achieve low DC-losses. The inductor was

designed in [8] and [1]. On the other hand, the 2 kW converter utilizes two pairwise coupled inductors with horizontal winding procedure for each half-bridge. The two inductors are in parallel so that DC-losses are reduced. The design was done in [3] and [2]. The coils of the two different inductors can be seen in Figure 3.
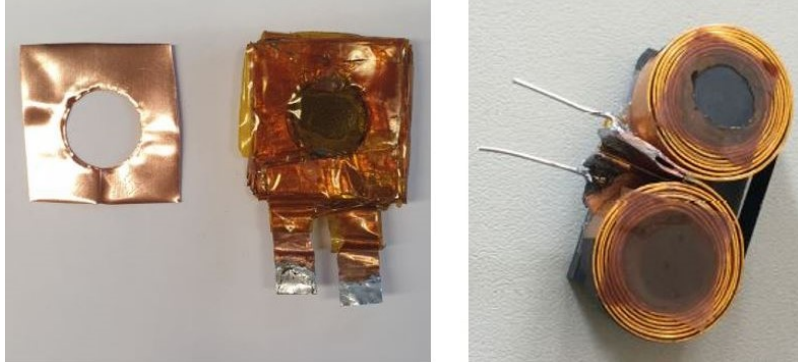
Figure 3: Inductor's coil for 1 kW converter (left) and for 2 kW converter (right) (image courtesy [1] [2])

- **MOSFETs**
  GaN MOSFETs are used in the 1-kW converter [13]. These MOSFETs have the advantage of high switching frequency and high current density. Therefore, the switching frequency of the 1 kW converter is 200 kHz. For the GaN MOSFETs, a 5 V gate drive is used which is lower than the recommended gate drive voltage of 6 V for optimal on-resistance. However, since a 5 V supply is already implemented for the control card, no further auxiliary regulator has to be introduced to obtain the gate drive voltage. On the other hand, the 2 kW converter contains Si-MOSFETs which are driven with a switching frequency of 100 kHz [14]. These MOSFETs have a lower on-resistance compared to the GaN MOSFETs. Another reason for using Si MOSFETs is their low price and easy availability. The gate drive voltage of the Si MOSFETs is 12 V, so an additional auxiliary regulator is introduced in the schematic of the 2 kW converter.

- **Control Card**
  The TMDSCNCD28335 control card based on the F28335 microcontroller is used for the 1 kW converter [16], whereas the TMDSDOCK28379D control card with the F28379D microcontroller is used for the 2 kW converter [17]. This new control card was introduced because the corresponding socket of the TMDSCNCD28335 is no longer available. While the TMDSCNCD28335 control card has only one CPU and one ADC, the new control card contains two CPUs and four ADCs, enabling a reduction of the execution time. Another advantage of the

TMDSDOCK28379D control card is the possibility to perform debugging via USB due to a USB-to-UART adapter on the control card. However, compared to the TMDSCNCD28335 control card the TMDSDOCK28379D control card has a much larger volume. The two control cards are shown in Figure 4.

Figure 4: TMS320F28335 control card of the 1 kW converter (left) and TMS320F28379D control card of the 2 kW converter (right)

2.3 POWER DENSITY

This section compares the two converters based on their power density. Power density is the amount of power handling capacity per unit volume.

At first, the power density of each converter prototype is calculated without taking into account the designed housing and the used heat sink. The power density and the volume of each converter is shown in Table 1. In this scenario, it is observed that the 2 kW converter has a lower power density compared to its counterpart.

	1 kW converter	2 kW converter
Power density in $\frac{kW}{dm^3}$	2.63	2.33
Volume in dm^3	0.38	0.86

Table 1: Power density of the converter prototypes (without housing and heat sink)

Various reasons can be found for the lower power density of the 2 kW converter:

- The lower power density and lower switching frequency of the Si-MOSFETs.

- The large volume of the TMDSDOCK28379D control card.

- The four pairwise coupled inductors require more space and larger footprints than the inductor of the 1 kW converter.

- An additional switching regulator is required to provide the 12 V gate drive voltage for the Si-MOSFETs. This voltage level is not needed for the 1 kW converter.

On top of that, the 1 kW converter has been optimized multiple times by previous project groups with the aim of maximizing power density. The 2 kW converter, on the other hand, is a first prototype.

The second scenario consists of calculating the power density of the converters along with their designed housing. This is shown in Table 2. Here, it is observed again that the 2 kW converter has a lower power density. The housing of the 1 kW converter was designed in [20] while the housing of the 2 kW converter was designed in [2]. The two housings are shown in Figure 5 and Figure 6.

	1 kW converter	2 kW converter
Power density in $\frac{kW}{dm^3}$	1.64	1.1
Volume in dm^3	0.61	1.81

Table 2: Power density of the converter prototypes (with designed housing)
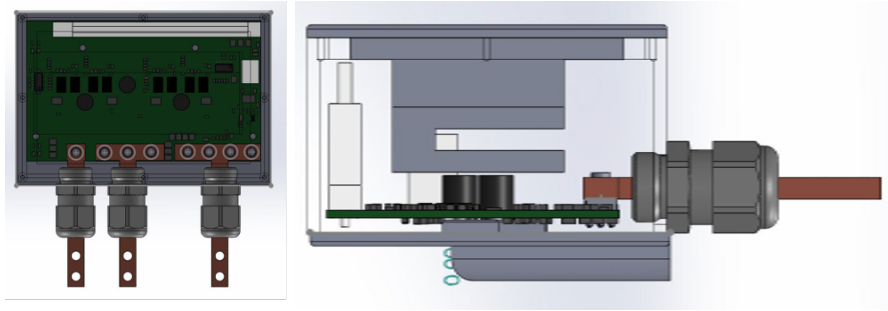
Figure 5: Designed housing of the 1 kW converter [20]
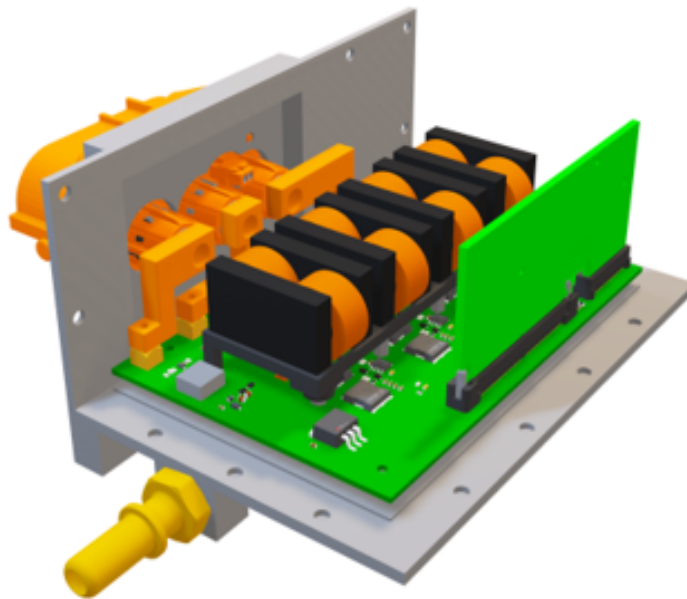
Figure 6: Designed housing of the 2 kW converter [2]

COMPARISON OF THE 1 KW AND 2 KW CONVERTER

To compare the performance of the two converters, measurements over the entire load range are recorded for both converters under equivalent measurement conditions which are ensured by using identical cooling systems. These cooling systems are described in a separate section. After that, the measurement setup and the measurement results are discussed.

3.1 COOLING CHAMBER

To ensure that an equivalent cooling system is used in the measurements for both converters, one cooling chamber (or pressure chamber) is manufactured for each converter by 3D printing. The cooling chamber for the 2 kW converter is shown in Figure 7. It is a housing with an opening whose width and height correspond exactly to the heat sink of the 2 kW converter. Two axial fans are mounted opposite the opening [10]. These fans provide an air flow which passes through the opening and actively cools the heat sink. During operation of the converter, the cooling chamber is placed directly next to the heat sink.

Figure 7: Cooling chamber of the 2 kW converter: The opening of the chamber is cut to fit the heatsink of the converter.

An identical cooling chamber is manufactured for the 1 kW converter. Only the dimensions of the opening differ from the cooling chamber for the 2 kW converter, as this is also the case for the heat sink. Both converters together with heat sink and cooling chamber can be seen in Figure 8.
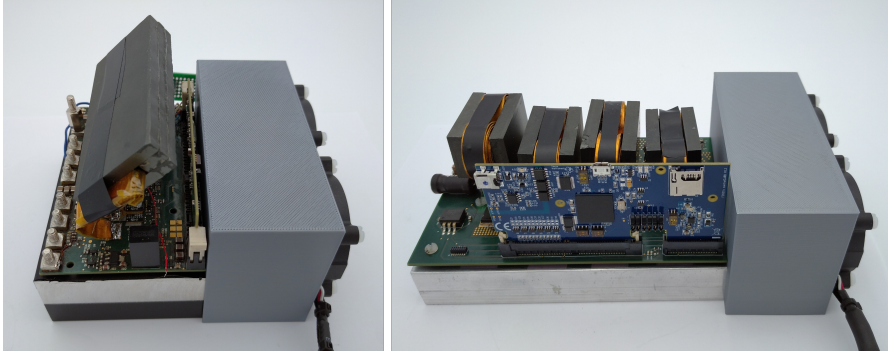
Figure 8: 1 kW converter (left) and 2 kW converter (right) with the corresponding 3D printed cooling chambers

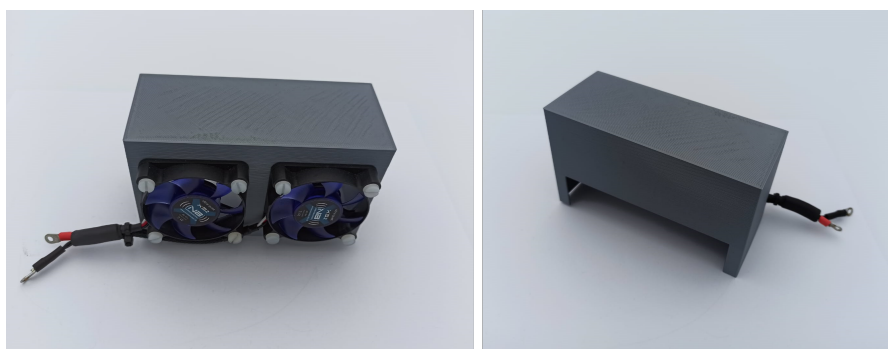By using the cooling chambers during the measurements, an equivalent cooling system with a defined distance is ensured for both converters. This makes the measurement results comparable with each other.

3.2 MEASUREMENT SETUP

The measurement setup in the lab is shown in Figure 9. The used converter is operated in buck mode. The input voltage $U_{\text{in}} = 48\,\text{V}$ is provided by an external power supply while the output voltage is set to $U_{\text{out}} = 12\,\text{V}$ by the control. An electronic load is connected to the output of the converter, through which the output current I_{out} can be adjusted. To record the values U_{in}, I_{in}, U_{out} and I_{out}, a power analyzer is used. While both voltages U_{in} and U_{out} can be measured directly by the power analyzer, current probes are required to measure the currents I_{in} and I_{out}. A schematic of the measured values can be seen in Figure 10. The input power $P_{\text{in}} = U_{\text{in}} \cdot I_{\text{in}}$, the output power $P_{\text{out}} = U_{\text{out}} \cdot I_{\text{out}}$ and the efficiency $\eta = \frac{P_{\text{out}}}{P_{\text{in}}}$ are calculated and recorded directly with the Power Analyzer.
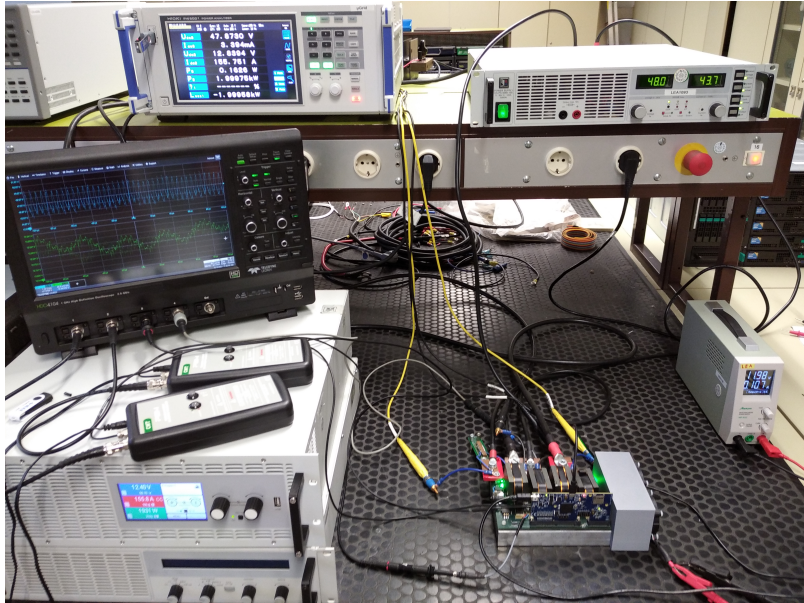
Figure 9: Measurement setup with the 2 kW converter in the lab
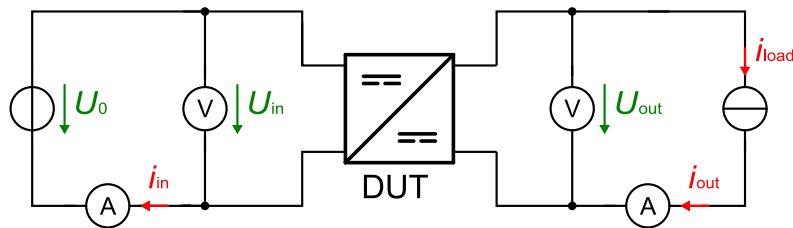
Figure 10: The basic measurement setup is identical for each converter as device under test (DUT)

Furthermore, an oscilloscope is used to measure U_{in} and U_{out} as functions of time. This allows the monitoring of the voltage ripples and of the control which sets the output voltage to $U_{\text{out}} = 12\,\text{V}$. The AC current of the rails 1 and 2 are also measured with Rogowski coils that are connected to the oscilloscope. The temperature of the converter is monitored with a thermal camera to ensure that critical component temperatures are not exceeded during operation. The measurement setup is identical for both converters.

The used devices are listed below:

- Power Supply EA-PS 9080-100 from EA [7]

- Electronic Load EA-EL 9080-510 B from EA [6]

- Power Analyzer PW6001 from HIOKI [12]

- Current Probe CT6845-05 from HIOKI [11]

- CWT Rogowski Current Waveform Transducer from PEM [19]

- Oscilloscope HDO4034A from Teledyne LeCroy [18]

- Thermal Camera from FLIR [9]

For the measurements, the converters are mounted on the corresponding heat sinks which are actively cooled by the matching cooling chamber. The supply voltage for the axial fans of the cooling chambers is provided by an additional external voltage source of 12 V.

To record measurements over the full load range of the converters, the electronic load is initially set to a current of $I_{out} = 0$. The output current I_{out} is then successively increased until the maximum output power of the respective converter is reached (1 kW and 2 kW). The measured values are recorded in 25 W steps with the power analyzer. As soon as the maximum output power is reached, the respective converter is operated at this power for one hour. Then the temperatures of the converter components are measured with the thermal camera.

3.3 MEASUREMENT RESULTS

3.3.1 *Efficiency*

The efficiency has been recorded by the power analyzer and is discussed in this section. Figure 11 shows the efficiency of both converters plotted as a function of the output power from 0 to 1 kW. The efficiency of the 2 kW converter over the entire load range (up to 2 kW) is shown in Figure 12.

The 1 kW converter reaches a maximum efficiency of 0.971 in the low load range at an output power between 200 W and 300 W. Subsequently, the efficiency drops as the output power increases. At the maximum output power of 1 kW, the efficiency is 0.939.
The maximum efficiency of the 2 kW converter is 0.965. The converter reaches it between 700 W and 800 W of the output power. At 1 kW, the efficiency is 0.964, whereas at the maximum output power of 2 kW, it is 0.955. The efficiency of the 2 kW converter is therefore more constant and the drop in efficiency is lower at higher loads than that for the 1 kW converter. However, the recorded average efficiency of the 2 kW converter is lower due to the poor performance in the low load range. A reason for the low efficiency at low load is that no optimization function is implemented in the 2 kW converter (see Chapter 5.2). Looking at higher loads, reasons for the higher efficiency of the 2 kW converter can be found in low switching and conduction losses

of the Si MOSFETs as well as in low ohmic losses of the pairwise coupled inductors.
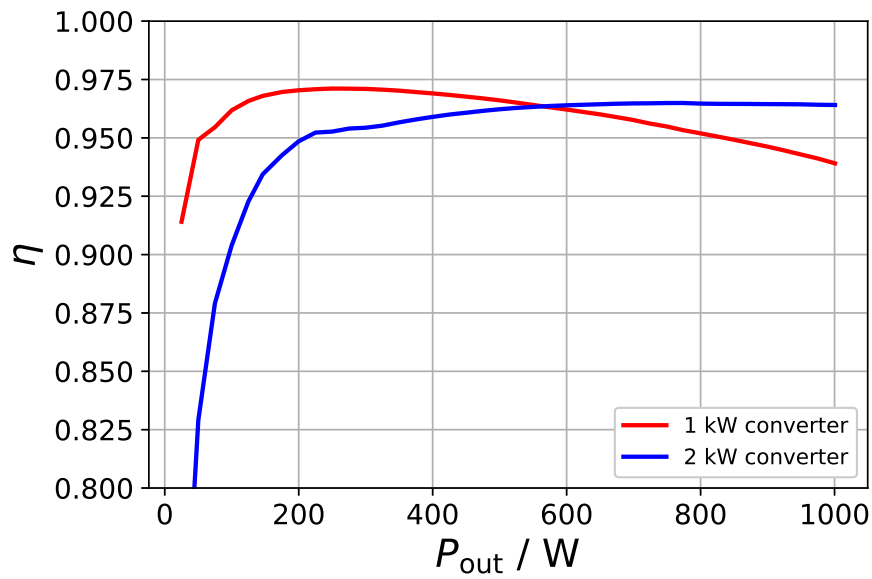

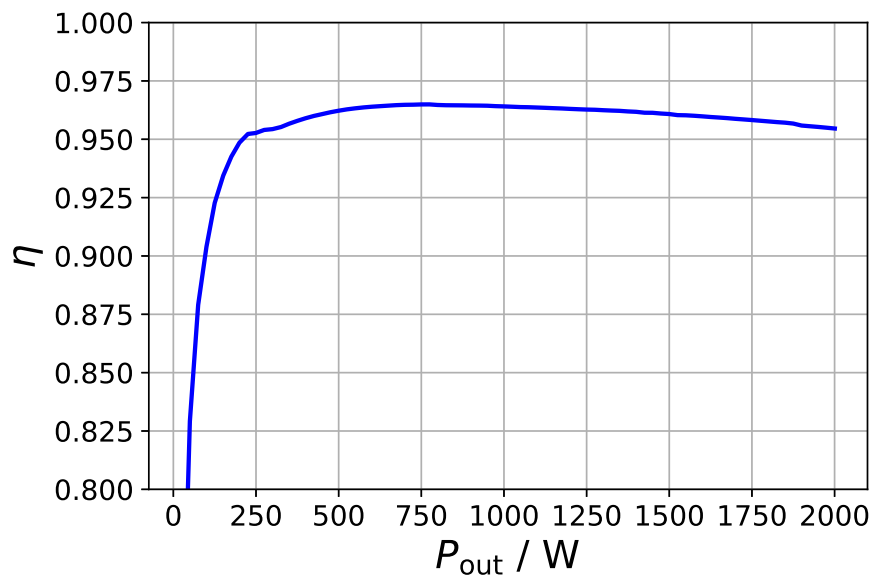Figure 11: Efficiency (η) vs output power (P_{out}) for both converters

Figure 12: Efficiency (η) vs output power (P_{out}) for the 2 kW converter

A tabular overview of the efficiency of the two converters can be found in Table 3.

	1 kW converter	2 kW converter
η_{max}	0.971	0.965
η_{avg}	0.959	0.953
η_{1kW}	0.939	0.964
η_{2kW}	-	0.955

Table 3: Efficiencies achieved by the 1 kW and 2 kW converter: Maximum, average, at 1 kW, at 2 kW

3.3.2 *Thermal profile*

The temperature measurements are taken after operating the converters at full load for one hour. The thermal profile is divided into the temperatures reached by different components of the converters. These components are:

- MOSFETs

- Inductors

- PCB material

In addition to that the average and the maximum temperature of the converters are recorded. Table 4 shows the measurement values for both converters. The corresponding FLIR images of the 1 kW converter are shown in Figure 13 and Figure 14, whereas the images of the 2 kW converter can be seen in Figure 15 and Figure 16.

Monitored temperature	1 kW converter	2 kW converter
MOSFET	81.1 °C	86.5 °C
Inductor	60.5 °C	78.3 °C
PCB	59.0 °C	70.2 °C
Average temperature	42.6 °C	58.8 °C
Maximum temperature	90.3 °C	96.1 °C

Table 4: Recorded temperatures of the 1 kW and 2 kW converter

For the 1 kW converter, a maximum temperature of 90.3 °C is reached at the winding of the inductor. The hottest GaN MOSFET reaches a temperature of 81.1 °C which is far from its critical temperature of 150 °C. The temperatures of the inductor (N95 ferrite) and the PCB material are also below their critical values. On the other hand, the 2 kW converter reaches a maximum temperature of 96.1 °C at the

solder pad of the rail 1 inductor. The hottest high side MOSFET has a temperature of 79 °C while the low side MOSFETs reach temperatures above 86 °C (shown in Appendix A). Overall, the average temperature of the 2 kW converter is significantly higher.

Figure 13: 1 kW converter: Temperature of MOSFET (1), Inductor (2) and PCB material (3)

Figure 14: 1 kW converter: Maximum temperature hotspot during full load operation
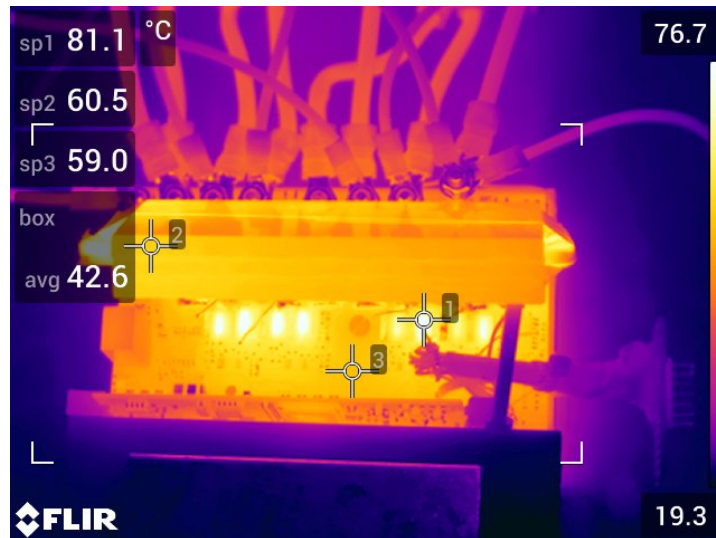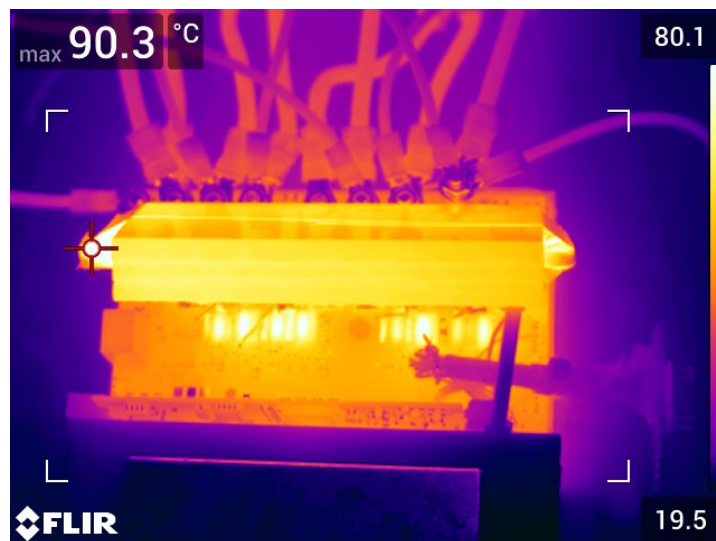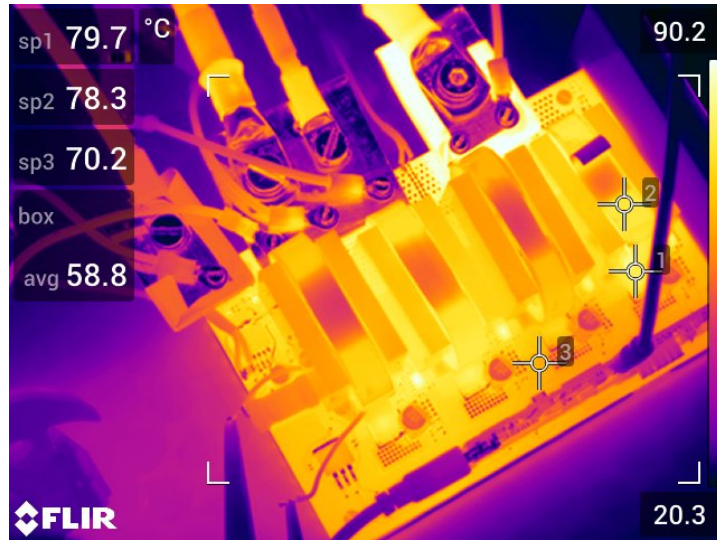
Figure 15: 2 kW converter: Temperature of MOSFET (1), Inductor (2) and PCB material (3)
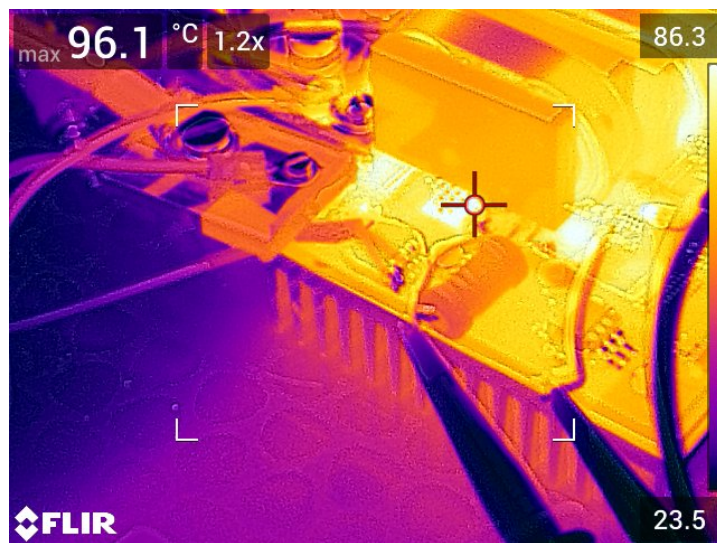

Figure 16: 2 kW converter: Maximum temperature hotspot during full load operation

DESCRIPTION OF THE HARDWARE ERRATA

Some hardware errors which could be identified during the assembly of the 2 kW converter were already discussed in [2]. During the testing of the converter in the context of this project, further errors have been identified. These errors are discussed in the following section. In addition, the applied workarounds are described.

4.1 POWER SUPPLY CIRCUIT

In the 2 kW converter schematic, an auxiliary buck switching regulator is used for providing the 12 V supply voltage for the gate drivers as shown in Figure 17. The component selection was done in [3], while the PCB design was finalized in [2]. The datasheet shows that an inductance value of 1.5 mH (0.5 A) is required for continuous conduction mode, so as to supply the gate drivers and further voltage regulators of the converter [15]. However, this value does not correspond to the inductance used in the PCB schematic, which is only 10 µH. The input and output filter capacitance used for the switching regulator do not match the recommendations in the data sheet either. The recommended component values can be taken from Table 5.

Component	Value in schematic	Recommended value
Inductor	10 µH	1.5 mH
Input capacitor	0.1 µF	>47 µF
Output capacitor	20 µF	100 µF - 470 µF

Table 5: Component values for use with the switching regulator

A new 1.5 mH inductor as well as the recommended electrolytic capacitor for the output capacitance have therefore been ordered. These components are glued to the PCB because their footprint does not match the PCB design. The components are then connected to the regulator circuit with solder and stranded wires. This workaround is shown in Figure 18.
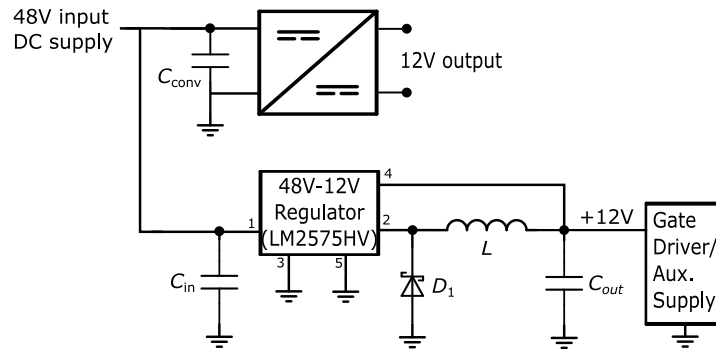
Figure 17: Auxiliary power supply schematic (in parallel with the converter)
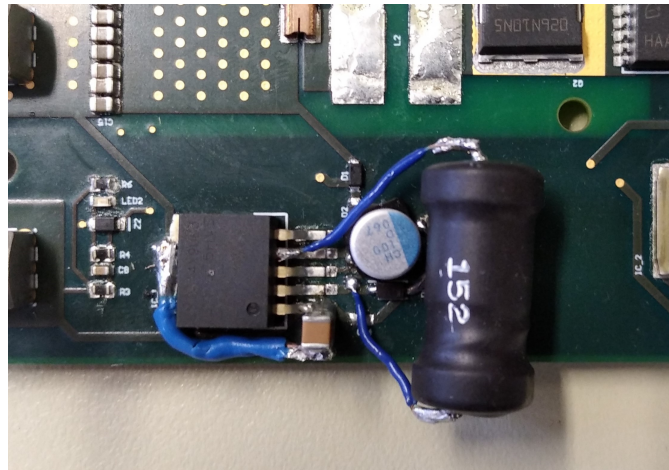
Figure 18: Soldered switching regulator with components glued to the PCB

Initially, an electrolytic capacitor was also used for the input capacitance of the regulator, as recommended in the data sheet. However, the use of the electrolytic capacitor resulted in an enormous temperature rise during operation (more than 120 °C at 500 W). A workaround to decrease the heating of the input capacitors is described in section 4.2.

4.2 INPUT CAPACITANCE

As per the schematic, the input capacitance required for the converter is 6.5 μF. This, however, does not align with the input capacitance requirement of the auxiliary regulator (48V-12V), which mandates a minimum capacitance of 47 μF. This issue along with insufficient inductance resulted in short circuit of the regulator.

One obvious solution to this problem is to increase the capacitance to a required level. An electrolytic capacitor of 47 μF was connected at the input of the regulator. But, that introduced another problem of heating of the capacitor during operation of the 2 kW converter

(more than 120 °C at 500 W). It was found that the capacitor was in parallel with the converter's input (see Figure 17). This parallel connection and a higher capacitance (with respect to converter's input capacitance of 6.5 μF) shifts all the current ripples to one electrolytic capacitor. As the ESR of an electrolytic capacitor is much higher as compared to a ceramic capacitor, the heat dissipation is also high. In short, one capacitor was in charge of regulator's and converter's ripple current.

The issue was overcome by connecting multiple ceramic capacitors (with small capacitance) in parallel, so as to distribute the current ripple. In addition to that, four electrolytic capacitors (of 33 μF) were connected at each rail, along with the ceramic capacitors with a total capacitance of 47 μF (shown in Figure 19). Thus increasing the total input capacitance to 179 μF. Moreover, a significant reduction of the input voltage ripple is also achieved by increasing the input capacitance.
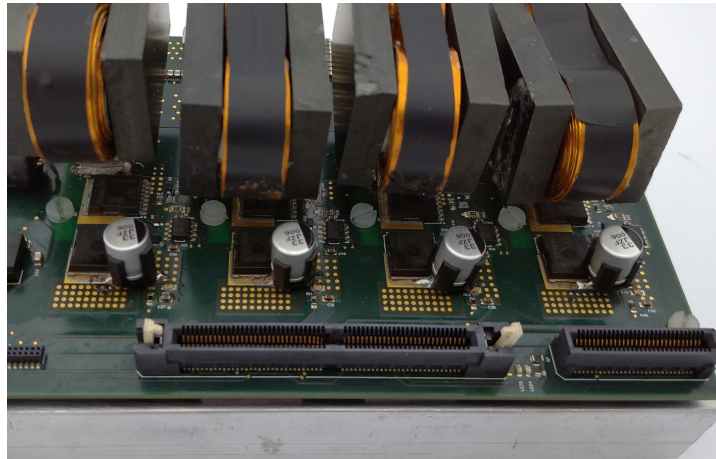
Figure 19: Soldered electrolytic capacitors at each rail to increase the input capacitance

4.3 GATE DRIVERS

The gate drivers experienced multiple short-cuts during the testing phase. Thus making them the most sensitive components on the board. The major cause of the problem was the over-voltage on the 12 V supply to the drivers as the absolute maximum rated supply voltage is limited to 20 V [21]. This over-voltage was caused due to the shortcut of the regulator and ripples in the output voltage (output voltage of 12 V is also connected to the output of the regulator so as to supply the board in case of boost mode operation).

Several solutions have been applied to safeguard the gate drivers. These are:

- Switch off converter in case of over-voltage at the output (software based solution).

- A 10 Ω series resistance is introduced at the input of the drivers, which together with the driver input capacitance of 1 µF acts as a low pass filter.

- A higher output capacitance (330 µF) is soldered at the regulator's output so as to reduce the voltage ripples.

For more safety, the diode connecting the converter's output voltage to the 12 V supply was removed. This ensures that no ripples superimpose on the 12 V supply line.

4.4 SOLDERING ISSUES

When testing the first rail, a soldering error was detected. Even if no PWM signals were sent from the control card, a voltage of 1 V to 5 V could be measured at the gate driver input pins HIN and LIN. These inputs correspond to the logic inputs for the high side and low side gate drive outputs. Since the logic '1' input of the driver corresponds to a voltage of 2.5 V or more, a reliable control of the first rail by PWM signals is not possible under these circumstances. As a cause for these voltages the control card socket has been identified, which most likely has not been soldered properly. As a workaround, a 10 kΩ pull-down resistor is soldered to each logic input.

Within the scope of this project, a second PCB of the 2 kW converter has been soldered with a soldering oven. This PCB does not show any errors like the one described. Using the soldering oven instead of soldering by hand can therefore be recommended for following projects.

OVERVIEW OF THE CONTROL SYSTEM

This chapter gives a short overview of the control structure used in the two converters. Though the control strategy employed in both the converters is same conceptually, there are few differences which are described in this chapter. Furthermore, an in depth explanation of the control algorithm can be found in [4] and in the project reports from SS18 [5] and WS19/20 [20].

5.1 CONTROL STRUCTURE

The topology used for controlling both the converters is an outer voltage control loop with an inner current control loop for each of the current rails. Figure 20 shows the control structure for the entire converter.

u^*_2 = Set output Voltage
$\bar{u}_2$ = Mean output Voltage
$\bar{u}_1$ = Mean input Voltage
$\bar{I}_{Lx}$ = Mean rail x current
$^*d_x$ = Duty cycle rail x
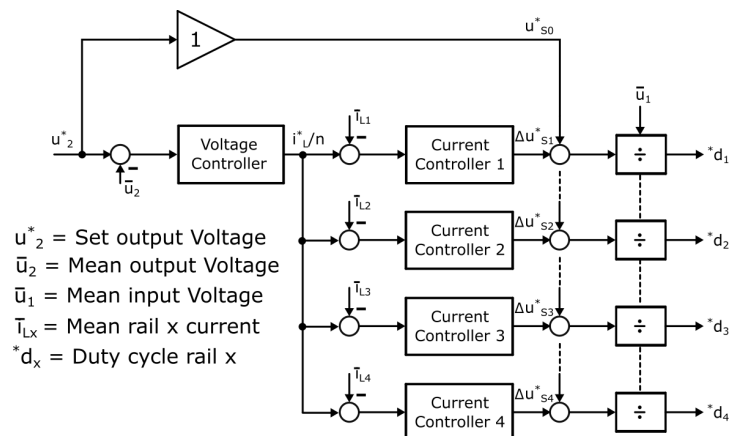
Figure 20: Block diagram of the four times interleaved cascaded control for the DC/DC converter

5.1.1 *Current Control-Loop*

The inner current control loop consists of only a proportional controller as there is no requirement of zero steady state error. The block diagram for the same is shown in Figure 21. The influence of the feed forward control, the output voltage and the voltage error can be put together into one disturbance quantity 'v'. The sampling period is described by $T_c = \frac{1}{f_{sw}}$, where f_{sw} denotes the switching frequency. A computational delay of one controller clock between current mea-

surement and PWM-update at the output of the current controller has been taken into account as per [5].

As the current controller consists of only proportional element, the transfer function of the controller is $G_{ci}(z) = K_{pc}$. Thus the overall current loop transfer function from the Figure 21 is

$$G_i(z) = \frac{\frac{K_{pc}T_c}{L}}{z^2 - z + \frac{K_{pc}T_c}{L}}$$
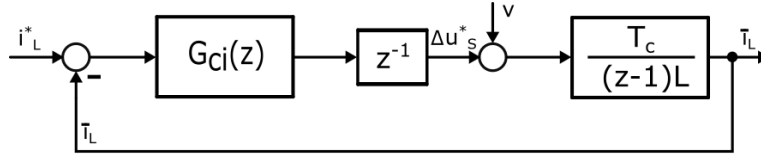
Figure 21: Current Control Loop

5.1.2 Voltage Control-Loop

The outer voltage controller consists of a PI (Proportional-Integral) controller. This is due to the fact that it is required to achieve perfect 12 V at the output. That is zero steady state error is required. As per [5] the outer voltage loop block diagram is shown in Figure 22.

Figure 22: Voltage Control Loop

The discrete time PI controller transfer function is given by

$$G_{cu}(z) = K_{pu} + K_{iu} \cdot \frac{T_c}{1 - z}$$

Adding this and the inner current loop transfer function gives us the overall closed loop transfer function denoted by

$$G_u(z) = \frac{G_{cu}(z)G_i(z)\frac{T_c}{(1-z)C_2}}{1 + G_{cu}(z)G_i(z)\frac{T_c}{(1-z)C_2}}$$

5.2 PROGRAMMING DIFFERENCES

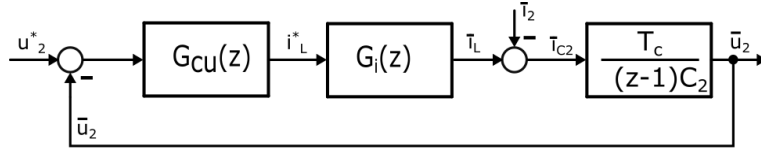Though basic structure of the control algorithm remains same in both the circuits, there are still some differences in the programming that differentiates the two. In addition to it, the use of different control cards also affects the implementation aspect to some degree.

There are four ADC modules in the TMS320F28379D (2 kW converter) as compared to TMS320F28335 (1 kW converter) which has only one such module. This makes the respective current measurement and duty cycle calculation modular and straight forward. As opposed to this, the 1 kW converter makes use of pointer address to ensure that the PWM unit responsible for the interrupt is determined. As there are some additional steps required in the interrupt function of the 1 kW converter, the execution time is little higher than that of 2 kW converter. This, however does not affect the overall converter control, as the duty cycle is not updated instantaneously but may affect for higher switching frequencies.

Another programming difference is due to the rail optimization function programmed in TMS320F28335 (1 kW converter) which optimizes the switching frequency and the number of active rails so as to achieve maximum efficiency at a given operating load. Such optimization is not programmed in TMS320F28-379D (2 kW converter). This operational strategy is further explained in [5]. A more detailed account of the hardware and software differences can be found in [2].

This project focuses on the assembly and testing of the 2 kW converter and its comparison with the 1 kW converter. There is a lot of room for improvement and extension of the firmware. For example a rail optimization function can be implemented and tested for the 2 kW converter as well. Also, the controller can be extended to include the discontinuous conduction mode (DCM) based on the operating point of the converter.

.

ABSTRACT

In this project, a comparison between the 1 kW and the 2 kW converter is performed. The assembly of the 2 kW converter is also finished as part of this project. The 1 kW converter has been assembled and tested by a previous project group.

Based on the work of the previous project groups, the assembly of the 2 kW converter is completed. This includes testing and debugging the hardware as well as manufacturing a heat sink and the pairwise coupled inductors. The control code is also put into operation. Further, a second board of the 2 kW converter is soldered.

For the comparison of the two converters, measurements are performed under equivalent measurement conditions which can be ensured by using similar cooling systems. During these measurements, the efficiency is recorded over the entire load range. For the comparison, the power density and the maximum component temperatures during operation are also considered. Chapter 2.3 shows that the 1 kW converter achieves a higher power density. This is especially due to the smaller control card size and the use of the GaN MOSFETs. Looking at the efficiency in Chapter 3.3, it can bee seen that the 1 kW converter achieves the highest efficiency. On average, the efficiency of the 1 kW converter is also higher than of the 2 kW converter. However, at higher loads, the 2 kW converter has a higher and more constant efficiency.
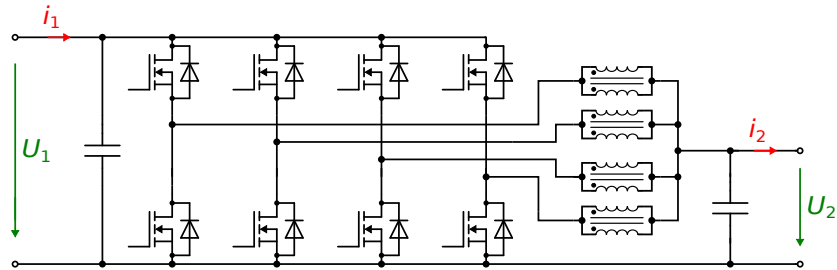
Figure 23: Topology of the 2 kW converter with pairwise coupled inductors, $U_1 = 48\,\text{V}$ and $U_2 = 12\,\text{V}$
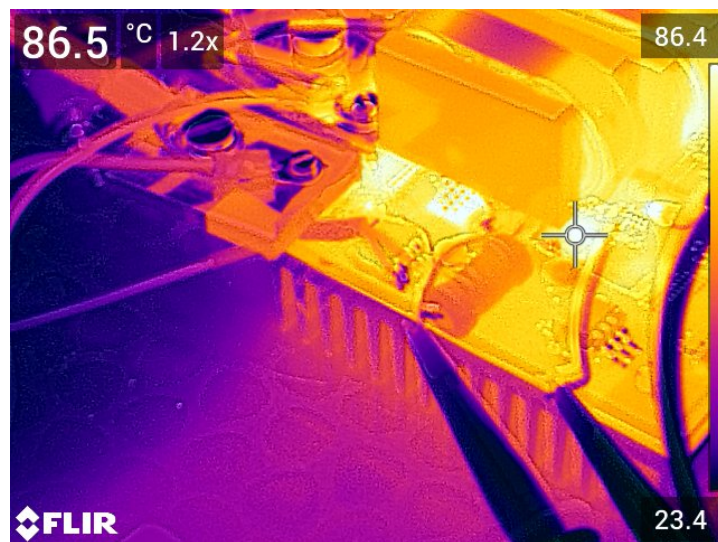

Figure 24: 2 kW converter: Temperature of the lowside MOSFET of rail one after one hour operation

BIBLIOGRAPHY

[1] Hendrik Becker, Christian von Germeten, Ismail Sarwar, and Hasnain Rajput. *Highly Compact 48 V-12V DC-DC Converter with Coupled Magnetics in Watercooled Housing for Automotive Applications*. Student Project, Paderborn, Deutschland, 2020.

[2] Marius Becker, Ishani Engineer, Jan Wiegard, and Denis Zeinel. *DESIGN OF A 4 TIMES INTERLEAVED 2 KW AUTOMOTIVE DC-DC CONVERTER*. Student Project, Paderborn, Deutschland, 2021.

[3] Sayantan Bhattacharjee, Ishani Engineer, Manuel Johannes Klaedtke, and Till Piepenbrock. *DESIGN OF A 4 TIMES INTERLEAVED 2 KW AUTOMOTIVE DC-DC CONVERTER*. Student Project, Paderborn, Deutschland, 2021.

[4] Prof. Dr.-Ing. Joachim Boecker. *Power Electronics*. Skript zur Vorlesung, Paderborn, Deutschland, 2020.

[5] Jannis Bohlmann, Niklas Gröne, Patrick Hosemann, Bastian Korthauer, Simon Gohlke, Stephane Donfack Sah, Daniel Urbaneck, Akash Singh, and Kibria Mahmud. *Highly Compact, Efficient 48 V-12 V DC-DC Converter for Vehicle Electrical Systems.* Student Project, Paderborn, Deutschland, 2018.

[6] EA Elektro-Automatik. *Datasheet EA-EL 9000 B SLAVE 7.2 kW*, 2018. URL https://elektroautomatik.com/shop/media/pdf/9e/97/0c/datasheet_el9000b_slave.pdf.

[7] EA Elektro-Automatik. *Datasheet EA-PS 9000 1U 1500 W & 3000 W*, 2018. URL https://elektroautomatik.com/shop/media/pdf/3f/8d/00/datasheet_ps9000_1u.pdf.

[8] Marius Fischer, Niklas Gröne, Suraj Joshi, Matthias Orth, and Robin Wolf. *Highly Compact, Efficient 48 V-12 V DC-DC Converter for Vehicle Electrical Systems with Coupled-Magnetics*. Student Project, Paderborn, Deutschland, 2019.

[9] FLIR. *Datasheet FLIR T500-SERIES*, 2021. URL https://flir.netx.net/file/asset/3929/original/attachment.

[10] Blacknoise Deutschland GmbH. *DC- Axialluefter/ Axial FAN - IT*, 2012. URL https://www.blacknoise.com/datas/downloads/datasheets/TData_BSF50_122012_de_en.pdf.

[11] HIOKI. *Datasheet CT6845 CT6845-05 AC/DC CURRENT PROBE*, 2018. URL https://www.hioki.com/global/products/current-probes/high-precision/id_6499.

[12] HIOKI. *Datasheet PW6001 POWER ANALYZER*, 2021. URL https://www.hioki.com/global/products/power-meters/power-analyzer/id_6029.

[13] GaN Systems Inc. *GS61008P Bottom-side cooled 100 V E-mode GaN transistor*, 2020. URL https://gansystems.com/wp-content/uploads/2020/09/GS61008P-DS-Rev-200402.pdf.

[14] Infineon. *IPT026N10N5 MOSFET OptiMOSTM 5 Power-Transistor, 100 V*, 2019. URL https://www.infineon.com/dgdl/Infineon-IPT026N10N5-DS-v02_01-EN.pdf?fileId=5546d46269e1c019016ac029615332f7.

[15] Texas Instruments. *LM1575/LM2575/LM2575HV SIMPLE SWITCHER 1A Step-Down Voltage Regulator*, 2013. URL https://www.ti.com/lit/ds/symlink/lm2575-n.pdf?ts=1639026871615&ref_url=https%253A%252F%252Fwww.google.com%252F.

[16] Texas Instruments. *TMS320F2833x, TMS320F2823x Digital Signal Controllers (DSCs)*, 2021. URL https://www.ti.com/lit/ds/sprs439p/sprs439p.pdf?ts=1639040535078&ref_url=https%253A%252F%252Fwww.google.com%252F.

[17] Texas Instruments. *TMS320F2837xD Dual-Core Microcontrollers*, 2021. URL https://www.ti.com/lit/ds/symlink/tms320f28377d-q1.pdf?ts=1639013820918.

[18] TELEDYNE LECROY. *Datasheet HDO4034A Oscilloscope*, 2019. URL http://cdn.teledynelecroy.com/files/pdf/hdo4000a-oscilloscopes-datasheet.pdf.

[19] Power Electronic Measurements Ltd. *Datasheet CWT Rogowski Current Waveform Transducer*, 2018. URL http://www.pemuk.com/Userfiles/CWT/cwt_0318.pdf.

[20] Till Piepenbrock, Dieter Teichrib, Manuel Johannes Klaedtke, and Konstantin Kroschewski. *REDESIGN OF A 1 KW AUTOMOTIVE DC-DC CONVERTER FOR INCREASED POWER DENSITY*. Student Project, Paderborn, Deutschland, 2020.

[21] International Rectifier. *IRS2011(S)PBF High and Low Side Driver*, 2015. URL https://www.infineon.com/dgdl/Infineon-IRS2011-DataSheet-v01_00-EN.pdf?fileId=5546d462533600a401535675c19f2784.